HOSTED BY

ELSEVIER

Available online at www.sciencedirect.com

ScienceDirect

Journal of Computational Design and Engineering 2 (2015) 129–136

www.elsevier.com/locate/jcde

Variational surface design under normal field guidance

Weidong Wu, Xunnian Yang*

Department of Mathematics, Zhejiang University, Hangzhou, China

Received 25 November 2014; received in revised form 4 December 2014; accepted 17 December 2014
Available online 9 March 2015

Abstract

This paper proposes a novel method for shape design of a Bézier surface with given boundary curves. The surface is defined as the minimizer of an extended membrane functional or an extended thin plate functional under the guidance of a specified normal field together with an initial prescribed surface. For given boundary curves and the guiding normal field, the free coefficients of a Bézier surface are obtained by solving a linear system. Unlike previous PDE based surface modeling techniques which construct surfaces just from boundaries, our proposed method can be used to generate smooth and fair surfaces that even follow a specified normal field. Several interesting examples are given to demonstrate the applications of the proposed method in geometric modeling.

Keywords: Membrane energy functional; Thin plate energy functional; Normal vector field; Geometric modeling

1. Introduction

Functional optimization technique is a general approach to fair surface design [1–4]. Moreton and Séquin [1] proposed a method for the creation of smoothly connected surfaces of any genus or topological type. Welch and Witkin [2] achieved fair surfaces by functional optimization of the surface shape. The users were able to control the surface shape by attaching points and curves to the surface. Fair surface design can also be formulated as solving partial differential equations (PDEs) subject to geometric or physical constraints [5–12]. In literature [6], a system was proposed for global and local deformations of PDE-based surface models subject to physical constraints. At the same time, the system also computed the B-spline finite element approximation of the PDE surface and allowed users to interactively manipulate the surface.

The tensor product Bézier surfaces, B-spline surfaces and NURBS surfaces are widely used in surface shape design. By employing the technique of control points, these surfaces can be designed interactively. Generally, the parametric surfaces can be deformed by searching the control points and weights subject to the geometric constraints [13–19]. Hu et al. [20] proposed two methods for modifying the shape of NURBS surfaces with geometric constraints, such as points, normal vectors at selected points, and pre-constructed curves. Both methods are dedicated to changing the control points and weights of an initial surface. Sauvage et al. [21] addressed the deformation of B-spline surfaces while constraining the volume enclosed by the surface. Pusch et al. [22] proposed an algorithm for locally deforming either a parametric surface or a hierarchical subdivision surface to match a set of positional and energy minimizing constraints.

Among all functionals for fair surface design, Dirichlet functional [23] and bi-harmonic functional [24] are popular for generating smooth and fair surfaces that interpolate given boundary curves. However, surfaces generated by these two functionals have few degrees of freedoms for shape adjustment, and they cannot represent even cylinder or cone like surfaces which are widely used in CAD. The geometric PDE method can generate typical surfaces for shape modeling [25] and surface restoration [26]. But, these equations are hard to have analytic solutions due to high nonlinearity. For applications like transition surface design or hole filling, the interpolating surfaces may have salient features which should

*Corresponding author.
E-mail addresses: wuweidong.happy@163.com (W. Wu), yxn@zju.edu.cn (X. Yang).
Peer review under responsibility of Society of CAD/CAM Engineers.

http://dx.doi.org/10.1016/j.jcde.2015.03.001

be controlled by additional parameters. This motivates us developing new functionals for fair surface design that have enough degrees of freedoms for shape adjustment as well as explicit solutions.

We propose to design Bézier surfaces with given borders by minimizing an extended membrane energy or an extended thin plate energy. Besides being as fair as possible, the resulting surface also fits to a prescribed normal vector field and an initial prescribed surface. Two shape parameters λ and γ are introduced to balance the effects of normal field and the initial surface. If λ and γ are chosen zero, the energy functional will degenerate to the Dirichlet functional or the bi-harmonic functional. The algorithm is easy to implement and the free control points of the surface are obtained by solving a linear system. For the convenience of adjusting the specified normal vector field, we can discretize the functional on a grid of parametric points and specify a discrete normal vector field. We have applied the proposed method for surface editing, hole filling and transition surface modeling.

The paper is organized as follows. In Section 2, an extended membrane energy functional and an extended thin plate energy functional are introduced. In Section 3, we propose explicit formulae for variational surface design under the guidance of normal vector field with given borders. Variational surface design under the guidance of discrete normal field is given in Section 4. In Section 5 we present several interesting examples. Section 6 concludes the paper.

2. Extended energy functionals for shape optimization

In this section, we propose two new energy functionals for Bézier surface shape design. These functionals are defined on the space of Bézier patches $\mathbf{R}:\Omega\to\Re^3$. Assuming $\mathbf{R}(u,v)=\sum_{i=0}^{n}\sum_{j=0}^{m}B_i^n(u)B_j^m(v)\mathbf{P}_{ij}$ is the Bézier surface to be designed, $\mathbf{N}(u,v)=\sum_{i=0}^{n_1}\sum_{j=0}^{m_1}B_i^{n_1}(u)B_j^{m_1}(v)\mathbf{N}_{ij}$ is the prescribed normal function and $\mathbf{S}(u,v)=\sum_{i=0}^{n}\sum_{j=0}^{m}B_i^n(u)B_j^m(v)\hat{\mathbf{P}}_{ij}$ is the given Bézier surface. We would like to find a fair surface $\mathbf{R}(u,v)$ that lies close to the given surface $\mathbf{S}(u,v)$ and fits well to the known normal field $\mathbf{N}(u,v)$.

First, we extend the membrane energy functional by allowing the surface to follow the shape of a given normal field and an initial surface. The extended membrane energy functional is given by

$$E_1(\mathbf{R})=\frac{1}{2}\int_\Omega\left\{\mathbf{R}_u^2+\mathbf{R}_v^2+\lambda\left[(\mathbf{R}_u\cdot\mathbf{N})^2+(\mathbf{R}_v\cdot\mathbf{N})^2\right]+\gamma(\mathbf{R}-\mathbf{S})^2\right\}du\,dv, \tag{1}$$

where $\mathbf{R}_u,\mathbf{R}_v$ are the partial derivatives of $\mathbf{R}$, and $\lambda(\geq 0)$, $\gamma(\geq 0)$ are the coefficients chosen by users. If $\lambda>0$, the resulting surface fits to the prescribed normals. If $\gamma>0$, the resulting surface follows the shape of the initial given surface also. The corresponding Euler–Lagrange equation of the functional is

$$0=(\mathbf{I}+\lambda\mathbf{N}\mathbf{N}^t)(\mathbf{R}_{uu}+\mathbf{R}_{vv})+\lambda[(\mathbf{N}\mathbf{N}_u^t+\mathbf{N}_u\mathbf{N}^t)\mathbf{R}_u+(\mathbf{N}\mathbf{N}_v^t+\mathbf{N}_v\mathbf{N}^t)\mathbf{R}_v]-\gamma(\mathbf{R}-\mathbf{S}),$$

where $\mathbf{I}$ is the identity matrix and t represents the transpose of a column vector. If both the coefficients λ and γ vanish, the functional reduces to the classical Dirichlet functional, and the corresponding Euler–Lagrange equation becomes the classical Laplacian equation.

Second, we extend the thin plate functional by using the prescribed normal field. In addition to interpolating the given boundary curves, the thin plate energy can be used to optimize surfaces that interpolate given tangent planes at the boundaries. In a similar fashion to the functional (1), the extended thin plate functional is defined as

$$E_2(\mathbf{R})=\frac{1}{2}\int_\Omega\left\{\mathbf{R}_{uu}^2+2\mathbf{R}_{uv}^2+\mathbf{R}_{vv}^2+\lambda[(\mathbf{R}_u\cdot\mathbf{N})^2+(\mathbf{R}_v\cdot\mathbf{N})^2]+\gamma(\mathbf{R}-\mathbf{S})^2\right\}du\,dv, \tag{2}$$

where $\mathbf{R}_{uu},\mathbf{R}_{uv},\mathbf{R}_{vv}$ are the second derivatives of $\mathbf{R}$. The corresponding Euler–Lagrange equation for this functional is

$$0=\mathbf{R}_{uuuu}+2\mathbf{R}_{uuvv}+\mathbf{R}_{vvvv}-\lambda\mathbf{N}\mathbf{N}^t\mathbf{R}_{uu}-\lambda\mathbf{N}\mathbf{N}^t\mathbf{R}_{vv}-\lambda[(\mathbf{N}\mathbf{N}_u^t+\mathbf{N}_u\mathbf{N}^t)\mathbf{R}_u+(\mathbf{N}\mathbf{N}_v^t+\mathbf{N}_v\mathbf{N}^t)\mathbf{R}_v]+\gamma(\mathbf{R}-\mathbf{S}).$$

When the coefficients λ,γ vanish, the functional degenerates to the thin plate functional. The corresponding Euler–Lagrange equation becomes the biharmonic equation.

3. Variational surface design with given borders

Though the minimizer of functional in Eq. (1) or in Eq. (2) can be characterized by the Euler–Lagrange equation, practical applications such as filling holes or designing transition surfaces usually need to solve fair surfaces with known boundaries. In the following we minimize the functional (1) or (2) by assuming the boundary curves or the boundary control points of a Bézier surface are already given. As the integrals in Eq. (1) or (2) can be computed explicitly, the free control points of the Bézier surface will be finally obtained by solving a linear system.

3.1. Surface modeling by minimizing the extended membrane energy

When we model a surface by minimizing the extended membrane energy functional with the given boundary curves, the minimization problem can be converted to solving the following system of equations.

$$\frac{\partial E_1}{\partial\mathbf{P}_{ij}}=0\quad(i=1,\ldots,n-1;j=1,\ldots,m-1).$$

Since the energy functional $E_1(\mathbf{R})$ is a quadratic functional in terms of the unknown control points, the mentioned equations form a linear system.

Let

$$\mathbf{C}_{kl}^{ij}=n^2\int_\Omega\{[B_{i-1}^{n-1}(u)-B_i^{n-1}(u)]B_j^m(v)B_k^{n-1}(u)B_l^m(v)(\mathbf{I}+\lambda\mathbf{N}\mathbf{N}^t)\}\,du\,dv,\quad k=0,1,\ldots,n-1,l=0,1,\ldots,m$$

and

$$\mathbf{D}_{kl}^{ij} = m^2 \int_{\Omega} \{B_i^n(u)[B_{j-1}^{m-1}(v) - B_j^{m-1}(v)]B_k^n(u)B_l^{m-1}(v) (\mathbf{I}+\lambda\mathbf{N}\mathbf{N}^t)\}\, du\, dv, \quad k=0,1,\ldots,n, l=0,1,\ldots,m-1$$

for $i \in \{1,\ldots,n-1\}$ and $j \in \{1,\ldots,m-1\}$, we have the following proposition.

Proposition 1. *A Bézier surface* $\mathbf{R}(u,v) = \sum_{i=0}^{n}\sum_{j=0}^{m} B_i^n(u) B_j^m(v)\mathbf{P}_{ij}$ *is the extremal of the functional (1) with prescribed border if and only if the control points of the surface satisfy the following linear system:*

$$0 = \sum_{k,l=0}^{n,m} (\mathbf{F}_{kl}^{ij} + \mathbf{G}_{kl}^{ij} + \mathbf{W}_{kl}^{ij})\mathbf{P}_{kl} - \sum_{k,l=0}^{n,m} \mathbf{W}_{kl}^{ij}\hat{\mathbf{P}}_{kl} \tag{3}$$

for any $i \in \{1,\ldots,n-1\}, j \in \{1,\ldots,m-1\}$, *where*

$$\mathbf{F}_{kl}^{ij} = \begin{cases} -\mathbf{C}_{0l}^{ij}, & k=0, \\ \mathbf{C}_{k-1,l}^{ij} - \mathbf{C}_{kl}^{ij}, & k=1,\ldots,n-1, \\ \mathbf{C}_{n-1,l}^{ij}, & k=n, \end{cases}$$

$$\mathbf{G}_{kl}^{ij} = \begin{cases} -\mathbf{D}_{k0}^{ij}, & l=0, \\ \mathbf{D}_{k,l-1}^{ij} - \mathbf{D}_{kl}^{ij}, & l=1,\ldots,m-1, \\ \mathbf{D}_{k,m-1}^{ij}, & l=m, \end{cases}$$

$$\mathbf{W}_{kl}^{ij} = \int_{\Omega} \gamma B_i^n(u)B_j^m(v)B_k^n(u)B_l^m(v)\, du\, dv\mathbf{I},$$

Proof. We compute the gradient of the functional with respect to each control point $\mathbf{P}_{ij}$. Denote $\Delta^{10}\mathbf{P}_{kl} = \mathbf{P}_{k+1,l} - \mathbf{P}_{kl}$ and $\Delta^{01}\mathbf{P}_{kl} = \mathbf{P}_{k,l+1} - \mathbf{P}_{kl}$. For any $i \in \{1,\ldots,n-1\}$, and any $j \in \{1,\ldots,m-1\}$, the gradient of functional E_1 is obtained as follows:

$$\begin{aligned}
\frac{\partial E_1}{\partial \mathbf{P}_{ij}} &= \int_{\Omega} \{n\left[B_{i-1}^{n-1}(u) - B_i^{n-1}(u)\right]B_j^m(v)\mathbf{R}_u \\
&\quad + mB_i^n(u)[B_{j-1}^{m-1}(v) - B_j^{m-1}(v)]\mathbf{R}_v \\
&\quad + \lambda n[B_{i-1}^{n-1}(u) - B_i^{n-1}(u)]B_j^m(v)\mathbf{N}(\mathbf{R}_u\cdot\mathbf{N}) \\
&\quad + \lambda mB_i^n(u)[B_{j-1}^{m-1}(v) - B_j^{m-1}(v)]\mathbf{N}(\mathbf{R}_v\cdot\mathbf{N}) \\
&\quad + \gamma B_i^n(u)B_j^m(v)(\mathbf{R}-\mathbf{S})\}\, du\, dv \\
&= \int_{\Omega} \{n[B_{i-1}^{n-1}(u) - B_i^{n-1}(u)]B_j^m(v)(\mathbf{I}+\lambda\mathbf{N}\mathbf{N}^t)\mathbf{R}_u \\
&\quad + mB_i^n(u)[B_{j-1}^{m-1}(v) - B_j^{m-1}(v)](\mathbf{I}+\lambda\mathbf{N}\mathbf{N}^t)\mathbf{R}_v \\
&\quad + \gamma B_i^n(u)B_j^m(v)(\mathbf{R}-\mathbf{S})\}\, du\, dv \\
&= n^2 \sum_{k,l=0}^{n-1,m} \int_{\Omega} \{[B_{i-1}^{n-1}(u) - B_i^{n-1}(u)]B_j^m(v) \\
&\quad B_k^{n-1}(u)B_l^m(v)(\mathbf{I}+\lambda\mathbf{N}\mathbf{N}^t)\}\, du\, dv\Delta^{10}\mathbf{P}_{kl} \\
&\quad + m^2 \sum_{k,l=0}^{n,m-1} \int_{\Omega} \{B_i^n(u)[B_{j-1}^{m-1}(v) - B_j^{m-1}(v)] \\
&\quad B_k^n(u)B_l^{m-1}(v)(\mathbf{I}+\lambda\mathbf{N}\mathbf{N}^t)\}\, du\, dv\Delta^{01}\mathbf{P}_{kl} \\
&\quad + \sum_{k,l=0}^{n,m} \int_{\Omega} \gamma B_i^n(u)B_j^m(v)B_k^n(u)B_l^m(v)\, du\, dv(\mathbf{P}_{kl} - \hat{\mathbf{P}}_{kl}).
\end{aligned}$$

By denoting the coefficient matrices in above equation as $\mathbf{C}_{kl}^{ij}$, $\mathbf{D}_{kl}^{ij}$ and $\mathbf{W}_{kl}^{ij}$, respectively, and further reformulating the differences $\Delta^{10}\mathbf{P}_{kl}$ and $\Delta^{10}\mathbf{P}_{kl}$, we obtain

$$\begin{aligned}
\frac{\partial E_1}{\partial \mathbf{P}_{ij}} &= \sum_{k,l=0}^{n-1,m} \mathbf{C}_{kl}^{ij}\Delta^{10}\mathbf{P}_{kl} + \sum_{k,l=0}^{n,m-1} \mathbf{D}_{kl}^{ij}\Delta^{10}\mathbf{P}_{kl} + \sum_{k,l=0}^{n,m} \mathbf{W}_{kl}^{ij}(\mathbf{P}_{kl} - \hat{\mathbf{P}}_{kl}) \\
&= \sum_{k,l=0}^{n,m} \mathbf{F}_{kl}^{ij}\mathbf{P}_{kl} + \sum_{k,l=0}^{n,m} \mathbf{G}_{kl}^{ij}\mathbf{P}_{kl} + \sum_{k,l=0}^{n,m} \mathbf{W}_{kl}^{ij}(\mathbf{P}_{kl} - \hat{\mathbf{P}}_{kl}) \\
&= \sum_{k,l=0}^{n,m} (\mathbf{F}_{kl}^{ij} + \mathbf{G}_{kl}^{ij} + \mathbf{W}_{kl}^{ij})\mathbf{P}_{kl} - \sum_{k,l=0}^{n,m} \mathbf{W}_{kl}^{ij}\hat{\mathbf{P}}_{kl}.
\end{aligned}$$

This leads the expression in Eq. (3). □

The linear system (3) can be written in the form of matrix equation, which takes the X, Y, Z coordinates of the control points as the unknowns. When the coordinates of all unknown control points are obtained, a fair surface that interpolates given boundary curves and fits the guiding normal field will be generated.

3.2. Surface modeling by minimizing the extended thin plate energy

Just like the thin plate energy functional, the extended thin plate energy functional permits the construction of surfaces with G^1 continuity with the surrounding surfaces. To achieve such a goal the outer two arrays of control points of a Bézier surface can be given in advance based on the continuity conditions while the remaining control points will be obtained by minimizing the functional (2) under the guidance of a given normal field. In a similar way to Section 3.1, we compute the control points where the gradient of the functional vanishes. From Eq. (2) we have

$$\begin{aligned}
\frac{\partial E_2}{\partial \mathbf{P}_{ij}} &= \int_{\Omega} \{n(n-1)[B_{i-2}^{n-2}(u) - 2B_{i-1}^{n-2}(u) + B_i^{n-2}(u)]B_j^m(v)\mathbf{R}_{uu} \\
&\quad + 2nm[B_{i-1}^{n-1}(u) - B_i^{n-1}(u)][B_{j-1}^{m-1}(v) - B_j^{m-1}(v)]\mathbf{R}_{uv} \\
&\quad + m(m-1)B_i^n(u)[B_{j-2}^{m-2}(v) - 2B_{j-1}^{m-2}(v) + B_j^{m-2}(v)]\mathbf{R}_{vv} \\
&\quad + \lambda n[B_{i-1}^{n-1}(u) - B_i^{n-1}(u)]B_j^m(v)\mathbf{N}(\mathbf{R}_u\cdot\mathbf{N}) \\
&\quad + \lambda mB_i^n(u)[B_{j-1}^{m-1}(v) - B_j^{m-1}(v)]\mathbf{N}(\mathbf{R}_v\cdot\mathbf{N}) \\
&\quad + \gamma B_i^n(u)B_j^m(v)(\mathbf{R}-\mathbf{S})\}\, du\, dv \\
&= 0
\end{aligned}$$

for $i \in \{2,\ldots,n-2\}$ and $j \in \{2,\ldots,m-2\}$.

Particularly, we let

$$\begin{aligned}
H_{kl}^{ij} &= \int_{\Omega} \{n^2(n-1)^2[B_{i-2}^{n-2}(u) - 2B_{i-1}^{n-2}(u) + B_i^{n-2}(u)]B_j^m(v) \\
&\quad B_k^{n-2}(u)B_l^m(v)\}\, du\, dv, \\
I_{kl}^{ij} &= \int_{\Omega} \{2n^2m^2[B_{i-1}^{n-1}(u) - B_i^{n-1}(u)][B_{j-1}^{m-1}(v) - B_j^{m-1}(v)] \\
&\quad B_k^{n-1}(u)B_l^{m-1}(v)\}\, du\, dv,
\end{aligned}$$

$$J_{kl}^{ij}=\int_{\Omega}\{m^2(m-1)^2B_i^n(u)[B_{j-2}^{m-2}(v)-2B_{j-1}^{m-2}(v)+B_j^{m-2}(v)]$$
$$B_k^n(u)B_l^{m-2}(v)\}\,du\,dv,$$
$$\mathbf{L}_{kl}^{ij}=\int_{\Omega}\lambda n^2[B_{i-1}^{n-1}(u)-B_i^{n-1}(u)]B_j^m(v)B_k^{n-1}(u)B_l^m(v)\mathbf{N}\mathbf{N}^t\,du\,dv,$$
$$\mathbf{M}_{kl}^{ij}=\int_{\Omega}\lambda m^2B_i^n(u)[B_{j-1}^{m-1}(v)-B_j^{m-1}(v)]B_k^n(u)B_l^{m-1}(v)\mathbf{N}\mathbf{N}^t\,du\,dv,$$
$$\mathbf{W}_{kl}^{ij}=\int_{\Omega}\gamma B_i^n(u)B_j^m(v)B_k^n(u)B_l^m(v)\,du\,dv\mathbf{I}.$$

The equation $\partial E_2/\partial\mathbf{P}_{ij}=0$ becomes

$$\begin{aligned}\frac{\partial E_2}{\partial\mathbf{P}_{ij}}&=\sum_{k,l=0}^{n-2,m}H_{kl}^{ij}\Delta^{20}\mathbf{P}_{kl}+\sum_{k,l=0}^{n-1,m-1}I_{kl}^{ij}\Delta^{11}\mathbf{P}_{kl}\\&\quad+\sum_{k,l=0}^{n,m-2}J_{kl}^{ij}\Delta^{02}\mathbf{P}_{kl}+\sum_{k,l=0}^{n-1,m}\mathbf{L}_{kl}^{ij}\Delta^{10}\mathbf{P}_{kl}\\&\quad+\sum_{k,l=0}^{n,m-1}\mathbf{M}_{kl}^{ij}\Delta^{01}\mathbf{P}_{kl}+\sum_{k,l=0}^{n,m}\mathbf{W}_{kl}^{ij}(\mathbf{P}_{kl}-\hat{\mathbf{P}}_{kl})\\&=\sum_{k,l=0}^{n,m}\overline{H}_{kl}^{ij}\mathbf{P}_{kl}+\sum_{k,l=0}^{n,m}\overline{I}_{kl}^{ij}\mathbf{P}_{kl}+\sum_{k,l=0}^{n,m}\overline{J}_{kl}^{ij}\mathbf{P}_{kl}\\&\quad+\sum_{k,l=0}^{n,m}\overline{\mathbf{L}}_{kl}^{ij}\mathbf{P}_{kl}+\sum_{k,l=0}^{n,m}\overline{\mathbf{M}}_{kl}^{ij}\mathbf{P}_{kl}+\sum_{k,l=0}^{n,m}\mathbf{W}_{kl}^{ij}(\mathbf{P}_{kl}-\hat{\mathbf{P}}_{kl})\\&=\sum_{k,l=0}^{n,m}(\overline{H}_{kl}^{ij}\mathbf{I}+\overline{I}_{kl}^{ij}\mathbf{I}+\overline{J}_{kl}^{ij}\mathbf{I}+\overline{\mathbf{L}}_{kl}^{ij}+\overline{\mathbf{M}}_{kl}^{ij}+\mathbf{W}_{kl}^{ij})\mathbf{P}_{kl}\\&\quad-\sum_{k,l=0}^{n,m}\mathbf{W}_{kl}^{ij}\hat{\mathbf{P}}_{kl}=0,\end{aligned}\tag{4}$$

where

$$\overline{H}_{kl}^{ij}=\begin{cases}H_{0l}^{ij}, & k=0,\\ H_{1l}^{ij}-2H_{0l}^{ij}, & k=1,\\ H_{kl}^{ij}-2H_{k-1,l}^{ij}+H_{k-2,l}^{ij}, & k=2,\ldots,n-2,\\ -2H_{n-2,l}^{ij}+H_{n-3,l}^{ij}, & k=n-1,\\ H_{n-2,l}^{ij}, & k=n,\end{cases}$$

$$\overline{I}_{kl}^{ij}=\begin{cases}I_{k0}^{ij}-I_{k-1,0}^{ij}, & k=1,\ldots,n-1,\ l=0,\\ I_{k-1,m-1}^{ij}-I_{k,m-1}^{ij}, & k=1,\ldots,n-1,\ l=m,\\ I_{0l}^{ij}-I_{0,l-1}^{ij}, & k=0,\ l=1,\ldots,m-1,\\ I_{n-1,l-1}^{ij}-I_{n-1,l}^{ij}, & k=n,\ l=1,\ldots,m-1,\\ I_{kl}^{ij}-I_{k-1,l}^{ij}-I_{k,l-1}^{ij}+I_{k-1,l-1}^{ij}, & k=1,\ldots,n-1,\\ & l=1,\ldots,m-1,\\ I_{00}^{ij}, & k=0,\ l=0,\\ -I_{0,m-1}^{ij}, & k=0,\ l=m,\\ -I_{n-1,0}^{ij}, & k=n,\ l=0,\\ I_{n-1,m-1}^{ij}, & k=n,\ l=m,\end{cases}$$

$$\overline{J}_{kl}^{ij}=\begin{cases}J_{k0}^{ij}, & l=0,\\ J_{k1}^{ij}-2J_{k0}^{ij}, & l=1,\\ J_{kl}^{ij}-2J_{k,l-1}^{ij}+J_{k,l-2}^{ij}, & l=2,\ldots,m-2,\\ -2J_{k,m-2}^{ij}+J_{k,m-3}^{ij}, & l=m-1,\\ J_{k,m-2}^{ij}, & l=m,\end{cases}$$

$$\overline{\mathbf{L}}_{kl}^{ij}=\begin{cases}-\mathbf{L}_{0l}^{ij}, & k=0,\\ \mathbf{L}_{k-1,l}^{ij}-\mathbf{L}_{kl}^{ij}, & k=1,\ldots,n-1,\\ \mathbf{L}_{n-1,l}^{ij}, & k=n,\end{cases}$$

$$\overline{\mathbf{M}}_{kl}^{ij}=\begin{cases}-\mathbf{M}_{k0}^{ij}, & l=0,\\ \mathbf{M}_{k,l-1}^{ij}-\mathbf{M}_{kl}^{ij}, & l=1,\ldots,m-1,\\ \mathbf{M}_{k,m-1}^{ij}, & l=m.\end{cases}$$

From Eq. (4) we know that the X,Y,Z coordinates of the unknown control points $\mathbf{P}_{ij}$ $(i=2,3,\ldots,n-2;j=2,3,\ldots,m-2)$ satisfy a system of linear equations. From the definition of the extended thin plate functional we know that the generated surface can interpolate the given boundary curves and the given tangent planes at the boundaries.

4. Variational surface design under discrete normal field guidance

An expected way to define the guiding normal field for the extended membrane energy functional or the extended thin plate energy functional is by using unit normals. However, the continuous unit normal field is generally represented by irrational functions which makes the integrals hard to compute. To balance the computational efficiency and unit normal requirement the functional (1) or (2) can be defined discretely. Instead of defining a continuous normal field we assume that unit normal vectors are given at a dense set of sampled grid points.

We now explain the main idea by computing the discrete integral for the extended membrane energy functional, the discrete integral for the extended thin plate functional can be computed in the same way. Assuming $\{N(u_{i_p},v_{j_p})\}_{i_p,j_p=0}^{n_p,m_p}$ are a set of unit normals corresponding to a set of points $\mathbf{S}(u_{i_p},v_{j_p})$, $u_{i_p}\in\{0,1/n_p,2/n_p,\ldots,1\}$, $v_{j_p}\in\{0,1/m_p,2/m_p,\ldots,1\}$ on the Bézier surface $\mathbf{S}(u,v)$. The functional (1) can be computed discretely as follows:

$$\begin{aligned}\hat{E}_1(\mathbf{R})=\frac{1}{2}\sum_{i_p,j_p=0}^{n_p,m_p}\Big\{&\mathbf{R}_u^2\Big(u_{i_p},v_{j_p}\Big)+\mathbf{R}_v^2\Big(u_{i_p},v_{j_p}\Big)\\&+\lambda_{i_p,j_p}((\mathbf{R}_u(u_{i_p},v_{j_p})\cdot\mathbf{N}(u_{i_p},v_{j_p}))^2\\&+\lambda_{i_p,j_p}((\mathbf{R}_v(u_{i_p},v_{j_p})\cdot\mathbf{N}(u_{i_p},v_{j_p}))^2\\&+\gamma_{i_p,j_p}(\mathbf{R}(u_{i_p},v_{j_p})-\mathbf{S}(u_{i_p},v_{j_p}))^2\Big\}.\end{aligned}\tag{5}$$

The weights λ_{i_p,j_p} and γ_{i_p,j_p} are non-negative numbers corresponding to the sampled normals $N(u_{i_p},v_{j_p})$ or sampled points $\mathbf{S}(u_{i_p},v_{j_p})$. These weights can be chosen as a same value or

different values for different normals or different points depending on various application purposes. Particularly, one can highlight surface features in some region by defining proper normal vectors $N(u_{i_p}, v_{j_p})$ and choosing large values for the weights λ_{i_p,j_p}. An example of preserving surface features based on normal constraint was given in [27].

With given boundary curves together with their control points, the objective functional $\hat{E}_1(\mathbf{R})$ is just the function of the inner control points of the Bézier surface. It follows that the free control points can be obtained by solving the following system:

$$\frac{\partial \hat{E}_1}{\partial \mathbf{P}_{ij}} = 0 \quad (i = 1, \ldots, n-1; j = 1, \ldots, m-1). \tag{6}$$

Let

$$\hat{\mathbf{C}}_{kl}^{ij} = n^2 \sum_{i_p,j_p=0}^{n_p,m_p} [B_{i-1}^{n-1}(u_{i_p}) - B_i^{n-1}(u_{i_p})] B_j^m(v_{j_p}) B_k^{n-1}(u_{i_p}) B_l^m(v_{j_p}) \times (\mathbf{I} + \lambda \mathbf{N}(u_{i_p}, v_{j_p}) \mathbf{N}^t(u_{i_p}, v_{j_p})),$$

$$\hat{\mathbf{D}}_{kl}^{ij} = m^2 \sum_{i_p,j_p=0}^{n_p,m_p} B_i^n(u_{i_p}) [B_{j-1}^{m-1}(v_{j_p}) - B_j^{m-1}(v_{j_p})] B_k^n(u_{i_p}) B_l^{m-1}(v_{j_p}) \times (\mathbf{I} + \lambda \mathbf{N}(u_{i_p}, v_{j_p}) \mathbf{N}^t(u_{i_p}, v_{j_p})).$$

Based on Eq. (6), the coordinates of the unknown control points $\mathbf{P}_{ij}$ $(i = 1, \ldots, n-1;\ j = 1, \ldots, m-1)$ satisfy the following linear system:

$$\sum_{k,l=0}^{n,m} (\hat{\mathbf{F}}_{kl}^{ij} + \hat{\mathbf{G}}_{kl}^{ij} + \hat{\mathbf{W}}_{kl}^{ij}) \mathbf{P}_{kl} - \sum_{k,l=0}^{n,m} \hat{\mathbf{W}}_{kl}^{ij} \hat{\mathbf{P}}_{kl} = 0 \tag{7}$$

for any $i \in \{1, \ldots, n-1\}, j \in \{1, \ldots, m-1\}$, where

$$\hat{\mathbf{F}}_{kl}^{ij} = \begin{cases} -\hat{\mathbf{C}}_{0l}^{ij}, & k = 0, \\ \hat{\mathbf{C}}_{k-1,l}^{ij} - \hat{\mathbf{C}}_{kl}^{ij}, & k = 1, \ldots, n-1, \\ \hat{\mathbf{C}}_{n-1,l}^{ij}, & k = n, \end{cases}$$

$$\hat{\mathbf{G}}_{kl}^{ij} = \begin{cases} -\hat{\mathbf{D}}_{k0}^{ij}, & l = 0, \\ \hat{\mathbf{D}}_{k,l-1}^{ij} - \hat{\mathbf{D}}_{kl}^{ij}, & l = 1, \ldots, m-1, \\ \hat{\mathbf{D}}_{k,m-1}^{ij}, & l = m, \end{cases}$$

$$\hat{\mathbf{W}}_{kl}^{ij} = \sum_{i_p,j_p=0}^{n_p,m_p} \gamma B_i^n(u_{i_p}) B_j^m(v_{j_p}) B_k^n(u_{i_p}) B_l^m(v_{j_p}) \mathbf{I}.$$

The system can be solved in the same way as in the previous section and a final surface that interpolates the given boundary curves will be generated.

5. Examples

In this section, we present a few examples to demonstrate the effects of surface shape design under normal field guidance. For each example we first construct an initial surface interpolating the given boundary curves, and then we design a guiding normal field for the surface. The final surface is obtained by solving the optimization problem. Besides the guiding normal field, the final surface can also be adjusted by changing the parameters λ and γ.

Fig. 1 illustrates an example of surface modeling by optimizing the extended membrane functional (1). An initial Bézier surface of order 5×5 is given with two different guiding normal fields; see Fig. 1(a) and (e) for the initial surface and the normal fields. By fixing the boundary curves and minimizing the energy functional with various choices of parameters λ and γ, we obtain several surface shapes shown as the remaining sub-figures of Fig. 1. From the figure we can see that the final surface follows the guiding normal field or the initial surface well when the parameter λ or γ has been increased, respectively.

In the following two figures we present examples of surface modeling under the guidance of discrete normal fields. Particularly, the parameter γ is chosen zero for these two figures.

Fig. 2(a) illustrates an initial Bézier surface of order 8×8. The prescribed normal field is drawn in red, as shown in Fig. 2(b). This is a hat shape with wave edge. Based on the initial Bézier surface and the prescribed normal field, we can edit the surface shape by choosing different values for the parameter λ when the extended membrane energy functional is minimized. Fig. 2(d)–(f) illustrates the surfaces obtained by choosing different values for the parameter λ but choosing zero for the parameter γ. Obviously, the top of the new hat is flat. As a comparison, the Bézier surface which minimizes the Dirichlet functional is given in Fig. 2(c).

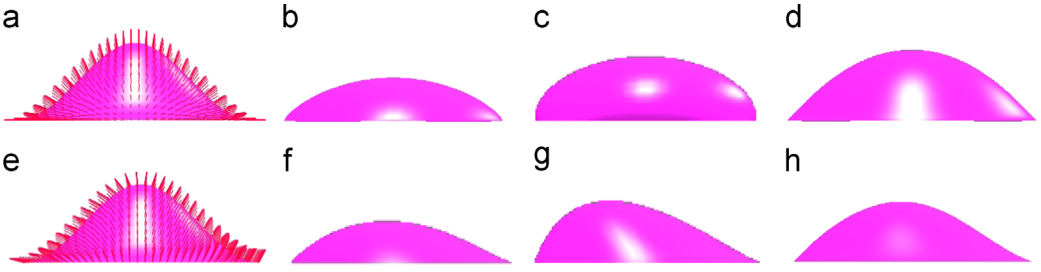

Fig. 1. Surface design by optimizing the extended membrane functional. Both top and bottom examples have the same initial surface but different prescribed normals. Top row (from left to right): initial Bézier surface and the prescribed normal function of order 8×8, optimized surfaces with parameters $(\lambda = 10, \gamma = 0)$, $(\lambda = 50, \gamma = 0)$, or $(\lambda = 10, \gamma = 200)$. Bottom row (from left to right): initial surface and the prescribed normal function of order 5×5, optimized surfaces with parameters $(\lambda = 10, \gamma = 0)$, $(\lambda = 50, \gamma = 0)$ or $(\lambda = 10, \gamma = 100)$.

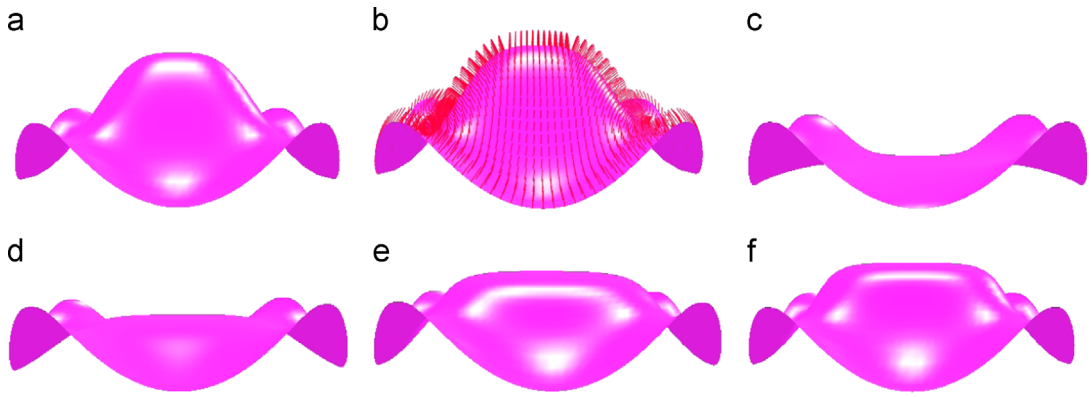

Fig. 2. Surface design by optimizing the discrete extended membrane energy functional. (a) The initial Bézier surface. (b) The initial surface with prescribed normals. (c) The extremal surface of the Dirichlet functional. (d) The optimized surface with parameters $\lambda = 1$ and $\gamma = 0$. (e) The optimized surface with parameters $\lambda = 10$ and $\gamma = 0$. (f) The optimized surface with parameters $\lambda = 50$ and $\gamma = 0$.

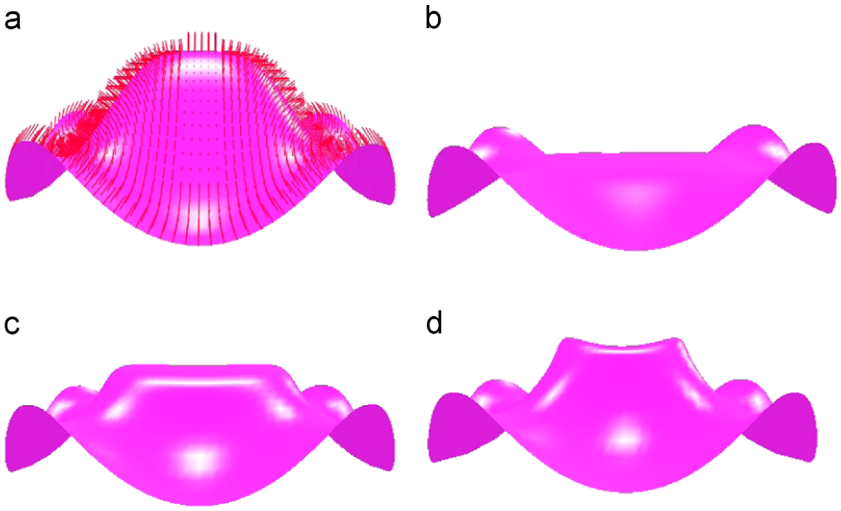

Fig. 3. Surface design by optimizing the discrete extended membrane energy functional. (a) The initial Bézier surface and the prescribed normal field. (b) The optimized surface with parameters $(\lambda = 10, \gamma = 0)$. (c) The optimized surface with parameters $(\lambda = 10, \gamma = 0)$. (d) The optimized surface with parameters $(\lambda = 50, \gamma = 0)$.

The initial surface illustrated in Fig. 3(a) is the same as the surface given in Fig. 2(a) but the prescribed normal field has been changed. The surfaces shown in Fig. 3(b)–(d) are generated by optimizing the discrete extended membrane energy functional with different choices of values for the parameter λ. For each figure the parameter λ is chosen the same value for all the sampled points. Clearly, the greater the value of λ is, the more obvious the feature of the resulting surface is.

Fig. 4 illustrates an example of hole filling by optimizing the thin plate functional or the extended thin plate functional. A hole with a set of surrounding patches is shown in Fig. 4(a) and we will fill the hole by a Bézier patch of degrees 7×7. To guarantee the G^1 continuity at the borders, the outer two arrays of control points are given in advance based on the border curves and the tangent planes at the borders. When we compute the remaining control points for the Bézier surface by minimizing the thin plate energy, a smooth interpolating surface is obtained; see Fig. 4(b) for the filling surface and Fig. 4(e) for the control mesh of the surface. If we set a guiding normal field for filling the hole, a Bézier surface that interpolates the given boundary data but minimizing the extended thin plate energy is obtained. Fig. 4(c) and (f) illustrates the filling surface and the control mesh of the surface, respectively. Comparing with the ground truth surface (Fig. 4(d)), the guiding normal field can help to restore salient features well.

Finally, we present two examples of blending surface modeling by optimizing the extended thin plate energy functional (2). For each example a bi-quintic Bézier surface is used as the transition surface between two given surfaces; see Fig. 5(a) and d for the initial surfaces. To guarantee the G^1 continuity between the transition surface and the surrounding surfaces, two arrays of boundary control points of the Bézier surface are given in advance. The surfaces generated by minimizing the thin plate energy are given in Fig. 5(b) and (e), respectively. From the figures we can see that the surfaces

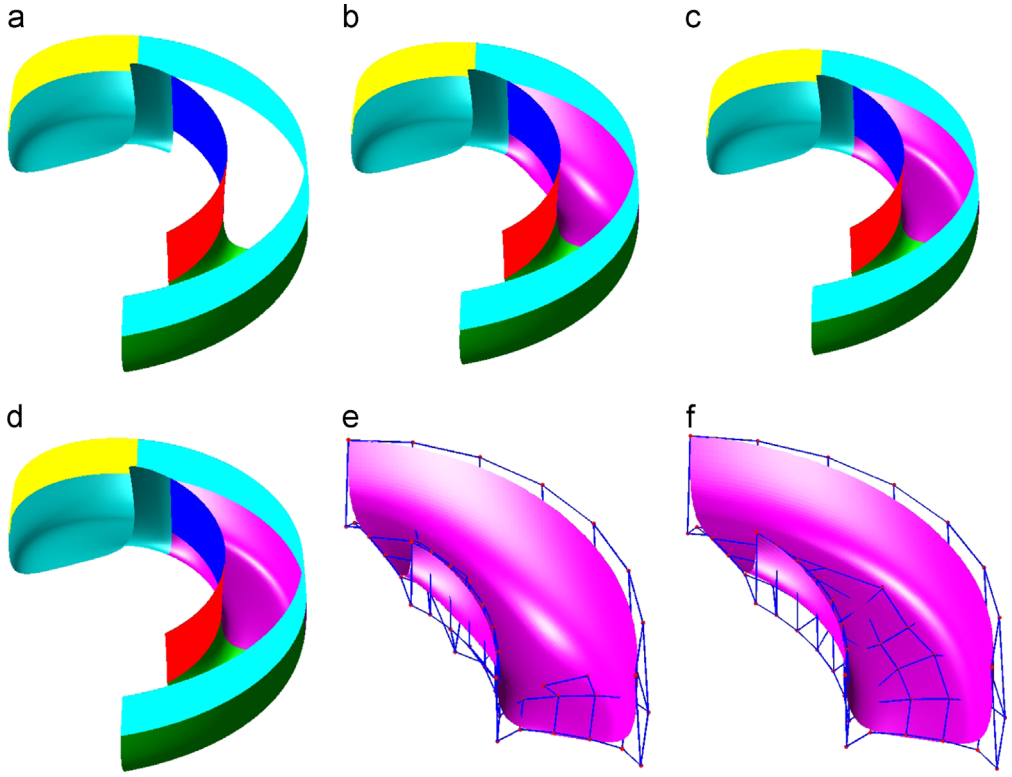

Fig. 4. Hole filling by optimizing the extended thin plate functional. (a) The hole with given boundary surfaces. (b) The filling surface (magenta) generated by optimizing the thin plate functional. (c) The filling surface by optimizing the extended thin plate functional ($\lambda = 500, \gamma = 0$). (d) The ground truth surface. (e) The close-up view of the filling surface in (b) together with the control mesh. (f) The close-up view of the filling surface in (c) together with the control mesh.

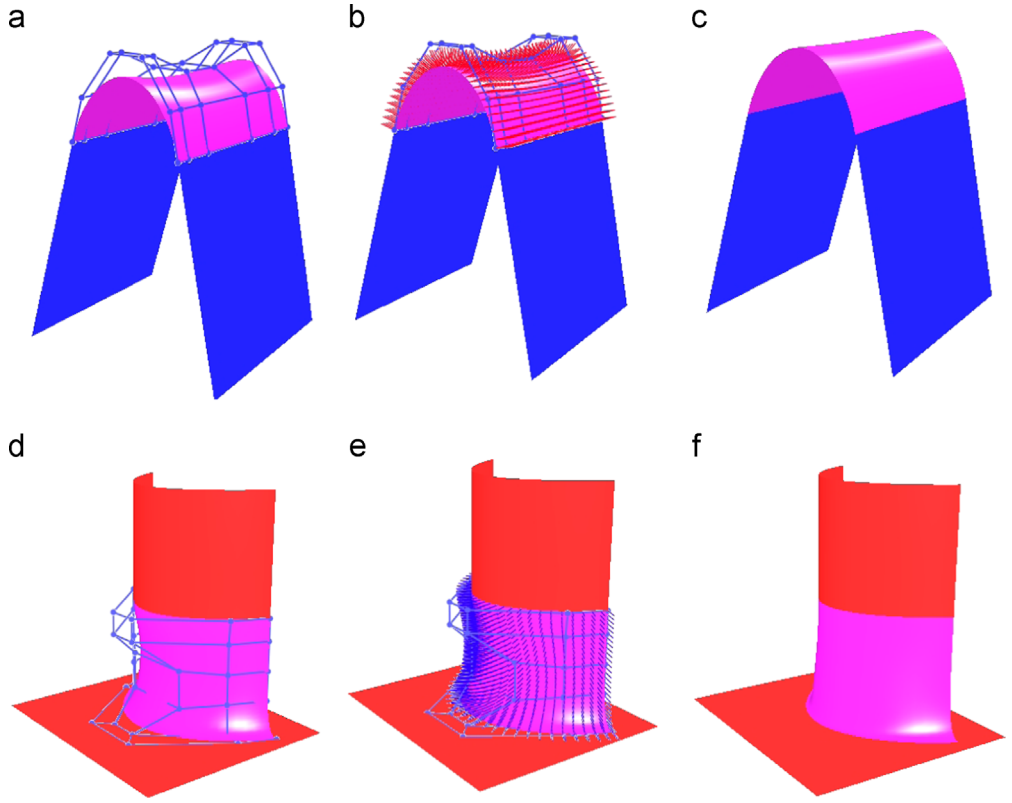

Fig. 5. Transition surface design by optimizing the extended thin plate functional. (a) and (d) Initial transition surfaces (in magenta) satisfying the boundary constraints. (b) and (e) The transition surfaces generated by optimizing the thin plate functional. The guiding normal vectors are also shown. (c) The transition surface generated by optimizing the extended thin plate functional with parameters $\lambda = 5$ and $\gamma = 0$. (f) The transition surface generated by optimizing the extended thin plate functional with parameters $\lambda = 500$ and $\gamma = 0$.

do not preserve the features well. When we add a guiding normal field for each surface and refine the surface to a new one by optimizing the extended thin plate energy, we obtain two surfaces following the surface features very well; see Fig. 5(c) and (f) for the obtained two transition surfaces.

6. Conclusion

In this paper, we have proposed two extended energy optimization models for surface shape design. Particularly, a surface can be designed or deformed by the extended membrane energy functional or the extended thin plate functional under the guidance of specified normal fields. The proposed method allows us to adjust the surface shape, while the discrete normal fields could be used for the local shape control with the increment of corresponding weights. When the surfaces and the guiding normal fields are represented by Bézier patches, the free control points of the Bézier surface can be obtained by solving a linear system. Besides the surface modeling purpose, the proposed method can be used for surface editing, hole filling and transition surface design, etc.

Conflict of interest statement

The authors declare no conflict of interest associated with this manuscript.

Acknowledgment

We owe thanks to reviewers for their helpful comments and suggestions. This work is supported by NNSF of China grants (11290142, 61272300).

References

[1] Moreton HP, Séquin CH. Functional optimization for fair surface design. In: Proceedings of ACM SIGGRAPH'92, vol. 26. 1992; p. 167–76.
[2] Welch W, Witkin A. Variational surface modeling. In: Proceedings of ACM SIGGRAPH'92, vol. 26. 1992; p. 157–66.
[3] Welch W, Witkin A. Free-form shape design using triangulated surfaces. In: Proceedings of SIGGRAPH'94. 1994; p. 247–56.
[4] Wang X, Cheng FF, Barsky BA. Energy and B-spline interproximation. *Computer-Aided Design* 1997;**29**:485–96.
[5] Du H, Qin H. Direct manipulation and interactive sculpting of PDE surfaces. *Computer Graphics Forum* 2000;**19**:261–70.
[6] Du H, Qin H. Dynamic PDE-based surface design using geometric and physical constraints. *Graphical Models* 2005;**67**:43–71.
[7] Zhang JJ, You LH. PDE based surface representation vase design. *Computers & Graphics* 2002;**26**:89–98.
[8] Zhang JJ, You LH. Fast surface modelling using a 6th order PDE. *Computer Graphics Forum* 2004;**23**:311–20.
[9] Du H, Qin H. A shape design system using volumetric implicit PDEs. *Computer Aided Design* 2004;**36**:1101–16.
[10] Xu G, Zhang Q. A general framework for surface modeling using geometric partial differential equations. *Computer Aided Geometric Design* 2008;**25**:181–202.
[11] Xu G. Mixed finite element methods for geometric modeling using general fourth order geometric flows. *Computer Aided Geometric Design* 2009;**26**(4)378–95.
[12] Huang WX, Wu HJL, Wang GJ. Constructing PDE-based surfaces bounded by geodesics or lines of curvature. *Computers & Mathematics with Applications* 2013;**65**:673–81.
[13] Feng J, Ma L, Peng Q. A new free-form deformation through the control of parametric surfaces. *Computers & Graphics* 1996;**20**:531–9.
[14] Hsu WM, Hughes JF, Kaufman H. Direct manipulation of free-form deformations. In: Proceedings of ACM SIGGRAPH'92, vol. 26. 1992; p. 177–84.
[15] Lamousin HJ, Waggenspack Jr WN. NURBS-based free-form deformations. *IEEE Computer Graphics and Applications* 1994;**14**:59–65.
[16] Michalik P, Kim DH, Bruderlin BD. Sketch-and constraint-based design of B-spline surfaces. In: Proceedings of the Seventh ACM Symposium on Solid Modeling and Applications. 2002; p. 297–304.
[17] Cheng F, Liu Z, Duan G, Yi B, Tan J. NURBS surface deformation design for complex products by transplanting the surface feature. *Engineering with Computers* 2014;**30**:599–608.
[18] Oya T, Amemiya H, Aoyama H, Higashi M. High-quality shape fitting for aesthetic modeling based on class a condition. *Computer Aided Design and Applications* 2014;**11**:632–9.
[19] Kineri Y, Endo S, Maekawa T. Surface design based on direct curvature editing. *Computer-Aided Design* 2014;**55**:1–12.
[20] Hu SM, Li YF, Ju T, Zhu X. Modifying the shape of NURBS surfaces with geometric constraints. *Computer Aided Design* 2001;**33**:903–12.
[21] Sauvage B, Hahmann S, Bonneau GP, Elber G. Detail preserving deformation of B-spline surfaces with volume constraint. *Computer Aided Geometric Design* 2008;**25**:678–96.
[22] Pusch R, Samavati F. Local constraint-based general surface deformation. In: Proceedings of the 2010 Shape Modeling International Conference. 2010; p. 256–60.
[23] Monterde J. Bézier surfaces of minimal area: *the Dirichlet approach*. *Computer Aided Geometric Design* 2004;**21**(2)117–36.
[24] Monterde J, Ugail H. On harmonic and biharmonic Bzier surfaces. *Computer Aided Geometric Design* 2004;**21**(7)697–715.
[25] Xu G, Zhang Q. G2 surface modeling using minimal mean-curvature-variation flow. *Computer-Aided Design* 2007;**39**(5)342–51.
[26] Clarenz U, Diewald U, Dziuk, G, et al. A finite element method for surface restoration with smooth boundary conditions. *Computer Aided Geometric Design* 2004;**21**(5)427–45.
[27] Imai Y, Hiraoka H, Kawaharada H. Quadrilateral mesh fitting that preserves sharp features based on multi-normals for Laplacian energy. *Journal of Computational Design and Engineering* 2014;**1**(2)88–95.